HHS Public Access

Author manuscript

Addit Manuf. Author manuscript; available in PMC 2022 April 01.

Published in final edited form as:

Addit Manuf. 2021 April ; 40: . doi:10.1016/j.addma.2021.101895.

Influence of random and designed porosities on 3D printed tricalcium phosphate-bioactive glass scaffolds

Susmita Bose[a,*], **Arjak Bhattacharjee**[a], **Dishary Banerjee**[a], **Aldo R. Boccaccini**[b], **Amit Bandyopadhyay**[a]

[a]W. M. Keck Biomedical Materials Research Laboratory, School of Mechanical and Materials Engineering, Washington State University, Pullman, WA 99164, USA

[b]Institute of Biomaterials, Department of Materials Science and Engineering, University of Erlangen-Nuremberg, Erlangen, Germany

Abstract

Calcium phosphate (CaP)-based ceramics are a popular choice for bone-graft applications due to their compositional similarities with bone. Similarly, Bioactive glass (BG) is also common for bone tissue engineering applications due to its excellent biocompatibility and bone binding ability. We report tricalcium phosphate (TCP)-BG (45S5 BG) composite scaffolds using conventional processing and binder jetting-based 3D printing (3DP) technique. We hypothesize that BG's addition in TCP will enhance densification *via* liquid phase sintering and improve mechanical properties. Further, BG addition to TCP should modulate the dissolution kinetics *in vitro.* This work's scientific objective is to understand the influence of random *vs.* designed porosity in TCP-BG ceramics towards variations in compressive strength and *in vitro* biocompatibility. Our findings indicate that a 5 wt % BG in TCP composite shows a compressive strength of 26.7 ± 2.7 MPa for random porosity structures having a total porosity of ~47.9%. The same composition in a designed porosity structure shows a compressive strength of 21.3 ± 2.9 MPa, having a total porosity of ~54.1%. Scaffolds are also tested for their dissolution kinetics and *in vitro* bone cell materials interaction, where TCP-BG compositions show favorable bone cell materials interactions. The addition of BG enhances a flaky hydroxycarbonate apatite (HCA) layer in 8 weeks *in vitro*. Our research shows that the porous TCP- BG scaffolds, fabricated *via* binder jetting method with enhanced mechanical properties and dissolution properties can be utilized in bone graft applications.

[*]Corresponding author. sbose@wsu.edu (S. Bose).

Data availability

Data will be made available upon request.

Declaration of Competing Interest

The authors declare that they have no known competing financial interests or personal relationships that could have appeared to influence the work reported in this paper.

Author statement

We declare that all authors have approved the submission of this revised version.

Appendix A. Supporting information

Supplementary data associated with this article can be found in the online version at doi:10.1016/j.addma.2021.101895.

Keywords

3D printing; *In vitro* dissolution; Bioactive glass; Scaffolds; Cytocompatibility

1. Introduction

Musculoskeletal disorders are among the most severe health concerns that affect many of the world's population [1,2]. The demand for skeletal reconstruction increases as more cases are performed yearly in the United States alone due to trauma, bone cancers, and other bone disorders, often addressed by bone grafting [3,4]. Autologous bone is considered the gold standard to treat small bone defects, but it is not a popular choice for repairing large-scale defects because of possible donor site complications [5]. Synthetic CaP-based ceramic scaffolds can be used as a bone graft, eliminating the possibility for donor-site morbidity, and can be made patient-specific and defect specific to treat small or large-scale bone defects [6,7]. Among biocompatible ceramics, CaP-based materials such as hydroxyapatite (HA) and tricalcium phosphate (TCP) can be considered as Nature's gift due to their chemical similarities with human hard tissues, which makes them an ideal choice for replacement surgeries [8–10]. Bioactive glasses (BGs) are also an important material for bone tissue engineering applications because of their excellent biocompatibility and biodegradability. The osteoconductive and osteoinductive properties of BGs can be tailored by changing the glass composition [11–13]. We hypothesize that the addition of a glassy material BG to TCP ceramic can enhance high-temperature densification *via* liquid phase sintering, which will result in higher sintered density and increase mechanical strength. The TCP-BG biphasic system will also show different biodegradation kinetics than pure BG or TCP.

Before choosing a material for bone tissue engineering, the desired application's performance need must be considered to achieve the best *in vivo* response. And sometimes, demanding performance needs may require a composite system than a single composition. For example, the slower degradation kinetics of bioactive TCP in the physiological system compared to BG can be utilized to tailor the dissolution properties of BG scaffolds to matching bone regeneration rates [14]. One of tissue engineering's current needs is to fabricate patient-specific porous scaffolds with biocompatible materials, providing temporary support for desired tissue repair and regeneration by accelerating cell proliferation and differentiation over the material surface [8,15,16]. The presence of porosity in the fabricated scaffolds is beneficial for biological fixation *in vivo* and nutrient supply to the newly formed bone. The mechanical properties of ceramic scaffolds are strongly influenced by the pore design, volume fraction, and pore shape [17]. 3D printing (3DP)-based advanced manufacturing technology can fabricate such patient-specific scaffolds with controlled pore architecture depending on the patient's defect-site scan. Based on the processing method and build parameter optimization, random and designed porosities can be obtained to tailor scaffolds' density and mechanical properties [18,19]. Poor mechanical properties may lead to implant failure *in vivo* due to pressure from the newly generated bone. Hence it is essential to tailor the material combination and process parameters to

manufacture scaffolds' comparable mechanical strength with the surrounding bone and desired degradation kinetics [20].

3D printed TCP-BG ceramic scaffolds using binder jetting can find potential applications in patient-specific musculoskeletal reconstructive surgeries. The 3D printed scaffolds are expected to show better compressive strength and control over dissolution kinetics, eliminating the requirement of a second surgery for autograft harvesting. However, due to previous limited works performed in this area [5,21], 3DP process parameter optimization and measurement of compressive strength as a function of composition, porosity, and degradation kinetics have been done as a part of this work. This study aims to understand the feasibility of fabricating TCP- BG scaffolds with designed and random porosity using the binder jetting method to measure the effects of composition on the mechanical properties, dissolution kinetics in psychological medium, and *in vitro* cytocompatibility. We hypothesize that BG's addition to TCP will enhance the dissolution rate of scaffolds compared to neat TCP and enhance the compressive strength. The 5 and 10 wt% of 45S5 BG (composition: 45 wt% SiO_2, 24.5 wt% CaO, 24.5 wt% Na_2O, and 6.0 wt% P_2O_5) were added to TCP to process TCP-BG composites. The binder jetting process parameter optimization was performed before porous scaffold fabrication. Scaffolds were sintered at high temperature followed by physical, mechanical, and biological characterizations.

2. Materials and methods

2.1. Powder synthesis and scaffolds fabrication

The pure β-TCP powder was prepared *via* solid-state synthesis, as described in our previous work [22]. Pure BG powder (45S5; composition: 45 wt% SiO_2, 24.5 wt% CaO, 24.5 wt% Na_2O, and 6.0 wt% P_2O_5) was commercially obtained (Schott, Germany) [23]. BG addition, 5 wt %, and 10 wt% in β-TCP, was done by ball milling both the powders thoroughly for 6 h in ethanol media using zirconia balls with the ball: powder: ethanol ratio of 3:1:1.5. After ball-milling, BG added TCP was washed thoroughly with deionized (DI) water followed by 72 h drying at 70 °C. The schematic of the powder preparation process is shown in Fig. 1a. Dried powders were pressed into a disc of 12.5 mm diameter and 2 mm thick using a uniaxial press at a pressure of 165 MPa with 5 min holding time. Pressed discs were sintered in a conventional furnace at 1250 °C for 2 h holding per our previous study [22].

A binder jet 3D printer (ExOne LLC, Irwin, PA, USA) was used to prepare TCP-BG scaffolds [19,22]. Scaffolds with different designs were fabricated to investigate the feasibility of preparing TCP-BG scaffolds by binder jetting. Fig. 1b shows the CAD models of different designs such as cylindrical scaffolds with 400 μm porosity, scaffold with corkscrew structure and no designed porosity, scaffold with ridges structure and no designed porosity, cylindrical scaffold without any designed porosity, and scaffold with a porous corkscrew structure. These scaffolds were designed using SolidWorks, converted to a *.stl* file, and fed into the printing system. A schematic of the binder jetting process is also shown in Fig. 1b. For detailed mechanical and biological characterizations, scaffolds of 11 mm height and 7 mm diameter with 400 μm designed interconnected porosity were used. Another set of scaffolds with random porosity was also fabricated using the same printer. Printing parameters were optimized to minimize defects and cracks, and an initial

foundation layer of 6 mm with a subsequent layer thickness of 40 μm was used for the fabrication. Similar printing parameters with a lower binder saturation were used for 5 wt% BG added TCP scaffolds. Green scaffolds were cured at 175 °C for 1.5 h. The loosely adhered extra powder particles from the cured scaffolds were removed using compressed air, and then scaffolds were sintered at 1250 °C for 2 h. Fig. 1c and d represent the optical microscopic images of all prepared green and sintered scaffolds, with various designs. Optical images showing the top views of green scaffolds are represented in Figs. S1, and S2 shows the top views of all sintered scaffolds. Samples were named TCP (100% TCP), TCP5BG (5 wt% BG added TCP), and TCP10BG (10 wt% BG added TCP) based on their compositions.

2.2. Phase, microstructural characterization, and mechanical properties

The phase purity of as-synthesized TCP and BG-added powders was characterized using the X-ray diffraction (Siemens D500 Diffractometer) in the 2θ range of 20– 20-60 degrees, and a step size 0.05 using Cu Kα radiation at 35 kV and 30 mA. The attenuated total reflection-infrared (ATR-IR) spectra were recorded on a Fourier transform infrared spectrometer (FTIR, Nicolet 6700, ThermoFisher, Madison, WI) range 400–1200 cm^{-1} to analyze changes in functional groups before and after TCP- BG dissolution studies. After the dissolution study, the surface morphology of the pressed scaffolds was analyzed using a field emission scanning electron microscope (FEI 200F, FEI Inc., OR, USA) at 5 kV, following a conductive layer of gold coating on the samples.

The bulk density (g/cm^3) of the scaffolds was calculated by measuring the geometrical dimensions and mass. The relative bulk density and total porosity (%) were calculated from the measured bulk density and the theoretical bulk densities. Archimedes' principle was used to measure the open porosity of the scaffolds according to ASTM B962 standards. Compressive strengths of the 3D printed scaffolds with random or designed porosity were measured per ASTM C773–88 standards using a screw-driven Instron universal testing machine with a constant crosshead speed of 0.033 mm/s.

2.3. Biological characterization

Uniaxially pressed disc samples were used for biological studies. A dissolution study of pure and BG added TCP discs was performed in simulated body fluid (SBF). The SBF solution was prepared per the method discussed in the published literature [24]. Prepared samples were immersed in a glass vial containing 5 mL SBF with a scaffold weight / SBF volume ratio of 0.11 g/cm^3 and incubated at 37 °C for a period of 1, 2, 4, and 8 weeks, keeping n = 3. SBF solution was changed every 3 or 4 days. After samples were taken out, they were dried at 60 °C for 72 h, followed by FTIR analysis.

Cytotoxicity assessment of prepared discs was performed using human osteoblast cells at 37 °C incubation in 5% CO_2 atmosphere. Human osteoblast cell lines, hFOB (PromoCell GmbH, Germany) with a density of 2×10^6 cells/mL were seeded on sterilized samples (autoclaved 121 °C for 60 min) by keeping the samples in 24 well plates. Per the recommendations of PromoCell, an osteoblast growth medium was used throughout the culture, and the medium was changed every 2 days during the study. MTT (3-(4,5-

dimethylthiazol-2-yl)-2,5-diphenyl tetrazolium bromide) assay was performed to measure cell viability after 3, 7, and 11 days of culture. All tests were done in triplicate. For analyzing cellular morphology by FESEM, samples were treated with 2% paraformaldehyde and 2% glutaraldehyde in 0.1 M phosphate buffer and refrigerated overnight at 4 °C. Room temperature fixation of the refrigerated samples was carried out for 1 h at ambient temperature using 2% osmium tetroxide (OsO_4) as the fixation media. Dehydration of the treated samples was performed in a standard ethanol series (30%, 50%, 70%, 95%, and 100% three times), accompanied by hexamethyldisilane (HMDS) drying. The HMDS treated samples were kept overnight in a desiccator for drying. Before FESEM, gold coating (thickness of 10–15 nm) was done using a sputter coater, and morphological analysis was performed through FESEM (FEI 200F, FEI Inc., OR, USA). Student's t performed statistical data analyses- test and p values < 0.05 or < 0.0001 were taken as a reference to conclude whether the obtained result is significant or extremely statistically significant, respectively.

3. Results

Table 1 shows detailed process parameter optimization using ExOne's binder jet 3D Printer. It can be seen that 40 μm layer thickness, 70% binder saturation, and 5 s drying time between printing each layer gave the best scaffolds. Fabricated scaffolds after each round of optimization are shown in Fig. S3.

Fig. 2 shows XRD patterns of sintered TCP, TCP5BG (5 wt% BG added TCP), and TCP10BG (10 wt% BG added TCP) powders. The presence of α-TCP (JCPDS 09–0348) and β-TCP (JCPDS 09–0169) in all samples are confirmed from the spectra. The presence of bioactive glass is also confirmed per published literature [23].

The ATR-IR spectra of TCP, TCP5BG, and TCP10BG are shown in Fig. 3a. BG added samples show functional groups, which are characteristics of both BG and TCP. Si−O−Si stretching modes in BG added samples are present at ~1100 cm^{-1}, which originates from BG addition [25,26]. O–P–O bending mode vibrations are detected in the range of ~500–620 cm^{-1}, common in both undoped TCP and BG added samples [27,28]. Fig. 3b–d presents ATR-IR spectra after dissolution studies in SBF, which shows that all samples show hydroxycarbonate apatite in the range 873–880 cm^{-1}, which is well supported by the available literature report [29].

SEM images after the dissolution study are shown in Figs. 4 and 5. It can be noted from Fig. 4 that the dissolution-precipitation leads to flaky apatite layer formation, which increases with BG addition [30]. Intense hydroxycarbonate apatite (HCA) layer is observed after 8 weeks of dissolution study, as shown in Fig. 5.

The bulk density (g/cm^3), relative bulk density (%), total and open porosity (%), designed porosity (%), and volume shrinkage (%) after sintering of the fabricated scaffolds are presented in Table 2. The highest bulk density of 1.6 ± 0.04 g/cm^3 is obtained for the TCP5BG composition with random porosity. This composition shows the highest volume shrinkage of ~13.7 ± 1.1% and the lowest total porosity of ~47.9 ± 0.03% compared to other compositions.

Compressive strength data are shown in Fig. 6, which shows that TCP with random porosity has a compressive strength of 8.4 ± 0.7 MPa, while 5 wt% BG addition leads to the improved compressive strength of 26.7 ± 2.7 MPa for the TCP5BG scaffolds with random porosity. However, the addition of BG beyond this level shows a detrimental effect on compressive strength, and the compressive strength for TCP10BG (with random pores) is 6 ± 0.9 MPa. Incorporation of designed porosity in TCP results in compressive strength of 5.6 ± 1.0 MPa (TCP with designed porosity). TCP10BG composition with interconnected designed porosity shows a compressive strength of 4.4 ± 1.5 MPa. In contrast, 21.3 ± 2.9 MPa compressive strength is obtained for the TCP5BG composition with 400 μm designed porosity.

Due to the best compressive strength of TCP5BG among the prepared compositions, TCP5BG is further analyzed for osteoblast cell viability *in vitro*. Osteoblast cell viability of selected samples after 3, 7, and 11 days of culture is shown in Fig. 7. Pure TCP is used as a control. Results show that BG addition to TCP up to the level 5 wt% remains cytocompatible.

4. Discussions

Patient-specific tissue engineering scaffolds can find applications in bone defect reconstruction surgeries and regenerative medicine [8]. The engineered architecture, interconnected porosity, functionalized surface, or a proper combination of materials with desired biological and mechanical properties not only helps in healthy tissue formation surrounding and inside the 3D printed scaffolds but also can provide the required biochemical atmosphere surrounding the new tissue, which allows nutrient supply, vascularization and helps in tissue growth [8,31,32]. The *in vivo* success of 3D printed scaffolds largely depends on the pore architecture and design [15,16,33]. A ceramic scaffold having the desired combination of mechanical and biological properties can be fabricated using the binder jetting technique, but it requires careful powder chemistry and build environment optimization to get the required product with controlled pore architecture [5,18,21]. We have successfully prepared TCP-BG scaffolds with five different designs (Fig. 1b–d). Our work proves the feasibility of fabricating TCP-BG scaffolds using the binder jetting technique. Layer thickness optimization is the most crucial step to achieve the desired mechanical strength of TCP-BG scaffolds. Shear stress arising between the layers during 3DP can easily break the single layers. Also, a too thick layer thickness results in poor bonding between the layers [5]. We have performed multiple process parameter optimizations (Table 1) to get the desired part. A layer thickness of 30 μm resulted in crumbled powder. After further optimizations, a layer thickness of 40 μm with a binder saturation of 40% gave the desired scaffolds for detailed characterization. Fig. 1 shows the binder jetting manufacturing technique to fabricate porous ceramic scaffolds used in this study. To ensure a defect and crack free part, detailed optimization of build parameters like the foundation layer, layer thickness, binder saturation, and maintaining proper powder chemistry, followed by depowderization and binder removal, are the essential steps for scaffold manufacturing [22,34]. In this study, after multiple trials and errors, we have used the layer thickness of 40 μm, followed by curing at 175 °C for 1.5 h. Our goal is to enhance the dissolution precipitation of β-TCP by adding BG. Fig. 3b–d presents the

ATR-IR spectra after the dissolution study in SBF. It is exciting to observe that even after only 1 week of dissolution studies, the TCP5BG and TCP10BG samples show a very weak hydroxycarbonate apatite (HCA) layer in the range ~873–880 cm^{-1} [29]. After 8 weeks, Dissolution reveals more intense HCA layers compared to week 1, which suggests enhanced dissolution precipitation compared to earlier time points.

Additionally, the most intense HCA bands are noticed in the sample TCP10BG due to the highest BG content compared to other compositions. Thus, ATR-IR is the primary evidence to suggest that BG addition significantly enhances TCP's dissolution precipitation rate. The faster dissolution kinetics and bioreactivity of BGs are well reported in the literature [12,35]. The enhancement of dissolution precipitation rate after BG addition is further confirmed using SEM, as presented in Figs. 4 and 5. Fig. 4 demonstrates a mild HCA layer formation after 1 and 2 weeks of dissolution studies, which increases with BG addition. The TCP10BG shows the most intense apatite layer formation among all these three compositions. A similar observation is also found after 4 and 8 weeks of dissolution. Hence, both the ATR-IR and SEM results indicate that BG addition accelerates the dissolution precipitation and HCA formation. This enhanced dissolution kinetics is essential to ensure complete resorbability of prepared scaffolds as partial resorbability of scaffolds inside the human body is detrimental for new bone formation and necessitates corrections through multiple surgeries [5]. Our group's previous work has revealed that as-synthesized TCP shows significant apatite layer formation after 12 weeks of dissolution in SBF, and the addition of dopants like Mg and Zn lowers the dissolution rate of TCP [36]. In contrast, current work shows that the addition of BG can enhance TCP dissolution. The interfacial tension between the scaffolds' solid surface and the existing aqueous medium plays a vital role in determining the composite's dissolution kinetics [14,37]. The water molecule replaces specific ions from the scaffold's surface during dissolution and the new complex dissolute into the bulk solution. Si and P's presence in the BG accelerates the dissolution process due to lower γ_{Sl} than only TCP [11,38].

Table 2 presents that the type of porosity, *i.e.*, random pores or designed pores, and the amount of BG addition significantly influence the bulk density, total porosity, and relative bulk density of the scaffolds. The samples with designed porosity show a lower bulk density as compared to the random porous counterpart. Fig. 6 presents the compressive strength of the prepared scaffolds. Interestingly, BG addition up to 5 wt% causes ~3–4 folds increase in the compressive strength compared to TCP for both random and designed porosity scaffolds. The addition of BG beyond this level shows a significant decrease in compressive strength. The compressive strength data corroborates well with observed bulk density data, as reported in Table 2. A significant increase in bulk density from 1 ± 0.06 g/cm^3 of pure TCP to 1.4 ± 0.05 g/cm^3 of TCP5BG is evident. The volume shrinkage data (Table 2) also supports this observation as the highest shrinkage is noticed in the case of TCP5BG. This significant increase in bulk density and compressive strength for TCP5BG is because of liquid phase sintering of the composite at 1250 °C. One previous work has reported a similar trend for hydroxyapatite – bioactive glass composites, which shows an increase of compressive strength from ~56 MPa to ~67 MPa due to 5 wt% BG addition [39]. The compressive strength enhancement by BG addition can be attributed to three critical factors (a) the sintering temperature, (b) composition of the bioactive glass, and

(c) amount of BG addition [40]. The 45S5 BG system shows a higher strength at higher sintering temperatures of ~1200–1300 °C, whereas a reverse trend has been observed for a two-oxide-based BG system [41]. Na's presence in 45S5 BG helps soften the TCP surface and acts as a glue to enhance densification during sintering. Besides, BG can stabilize the β-TCP phase by hindering the $\beta \rightarrow \alpha$ transformation [40,41]. In contrast, the increasing amount of BG causes phosphorous replacement present in β - TCP with Si within the lattice, and this substitution reaches saturation at ~5–7.5 wt% BG addition. Addition of BG beyond this level results in excess Si in the composite system and more undesirable liquid phase formation, which hinders TCP densification and causes detrimental effects to the compressive strength [41,42]. The liquid phase sintering after BG addition also helps crack-bridging and crack-deflection, which are two contributing factors towards enhanced compressive strength. Partial crystallization of BG at higher sintering temperatures may reduce bioactivity by slowing down the apatite formation layer. Crystallinity up to 40% does not show any detrimental effects on bioactivity. Optimizing the sintering cycle is the essential factor to determine the compressive strength of BG added scaffolds, and a two-step sintering process offers better compressive strength [43,44]. The total porosity and obtained compressive strength were correlated by power-law fit. Eqs. (1) and (2) present the fit for scaffolds with random and designed porosity, respectively (n = 6).

$$Y = 2(X)^{-4 \cdot 076} \times 10^{8} \quad (1)$$

$$Y = 5(X)^{-6 \cdot 553} \times 10^{12} \quad (2)$$

In the above equations, Y is compressive strength in MPa, and X is the total porosity (%). The R^2 values of Eqs. (1) and (2) are 0.98 and 0.99, respectively. The theoretical compressive strength values of samples with random and designed porosities are presented in Table 2 as calculated strength. For the TCP5BG samples, the theoretically expected strength with random porosity is 54.4 MPa based on Eq. (2), but experimentally this sample set shows a compressive strength of 26.7 MPa. In contrast, the theoretical compressive strength of TCP5BG with designed porosity is 16.1 MPa based on Eq. (1), and experimentally the sample shows a higher strength of 21.3 MPa. Our data indicate that incorporating designed porosity during 3D printing of TCP-BG scaffolds leads to higher compressive strength than the theoretically expected value. Further addition of BG in the sample with designed or random porosity shows a reduction in compressive strength. In a previous study [45], authors have shown that different processing parameters in Fused deposition modeling (FDM) significantly influence the porosity and mechanical properties of the fabricated acrylonitrile-butadiene-styrene (ABS) scaffolds. Among all the processing parameters, air gap and raster-width are the most important factors in FDM, determining the porosity and compressive strength of scaffolds. Another study [46] shows, different scaffold architecture and porosity influence the compressive stiffness. Scaffolds with a compressive stiffness gradient are feasible *via* selective laser sintering (SLS). The obtained porosity-stiffness relationship follows a linear trend, and the experimental value of the equation constant is 15% lower than the theoretical one. This drop is attributed to the nature of the SLS, and the imperfection presents in the parts. Hence, the specific

3D printing method, scaffold material, and processing parameters all play an important role in determining the porosity and mechanical properties of obtained scaffolds. In the current work, we have performed several process optimizations (Table 1), and the optimized parameter is utilized for printing all compositions and structures, which eliminates other processing related factors, which can influence the mechanical properties of the scaffolds. Our data shows a combination of design modifications during 3DP and BG addition up to 5 wt% results in a compressive strength increase for the 3D printed TCP-BG composites.

Fig. 7a shows the MTT assay results with osteoblast cells up to day 11, and both the control TCP and TCP5BG show similar cytocompatibility. As per ISO 10993 protocol, BG addition did not cause any cytotoxic effects due to the presence of Si and other ions from the composite. MTT assay indicates that cell viability significantly increases at day 11 compared to earlier time points for both the control and TCP5BG sample, indicating *in vitro* osteogenic potential of the fabricated scaffolds. The SEM image in Fig. 7b shows the presence of healthy osteoblast cells in TCP5BG. Our group's previous work indicates that the presence of porosity on the 3D printed scaffold surface helps in osteoblast attachment compared to the dense scaffolds [22]. In a recent work [33], we have demonstrated that porosity, and surface topography 3D printed scaffolds play an important role on cell morphology, and proliferation. In addition, finer microstructure and micropores can enhance osteoblast proliferation and apatite formation on the scaffold surface [47,48]. However, due to enhanced dissolution and apatite layer formation, the cells are covered with a flaky HCA layer [36]. Our results establish that 45S5 BG added TCP is ideal for manufacturing patient-specific scaffolds with designed or random porosity. Additionally, the cytocompatibility and optimum mechanical properties of these composites are dependent on the level of BG addition. In previous works by our group [17,49], we have reported that 3D printed scaffolds with interconnected designed porosity resulted in better *in vivo* bone formation and tissue in-growth after incorporating different additives. Hence, future studies may include comparing the *in vivo* bone formation ability of TCP-BG scaffolds with random or designed porosities, respectively. Utilization of this composition in 3D bioprinting using collagen inks for better tissue integration and investigation of the chemical and biological properties of 3D printed transition metal-doped TCP-BG scaffolds are other possible areas for future research [12,50,51].

5. Conclusions

This study shows the feasibility of utilizing TCP-BG composite to fabricate 3D printed scaffolds with different designs. These scaffolds possess controlled dissolution kinetics and higher mechanical strength. The effects of 45S5 BG addition on increasing the dissolution kinetics of TCP scaffolds are observed by dense apatite layer formation even at early time points of 2 and 4 weeks compared to pure TCP as control. The scaffolds' highest compressive strength is noticed for the composition of 5 wt% BG added TCP for both random and designed porosity scaffolds. The incorporation of designed porosity leads to an increase in compressive strength for the TCP5BG composition than the theoretically obtained value. The TCP5BG composition is cytocompatible with hFOB cells. BG addition to 10 wt% shows a detrimental effect on the compressive strength of the scaffolds. Our

findings indicate that 3D printed TCP-45S5 BG composite scaffolds possess an optimum combination of bioactivity, compressive strength, and cytocompatibility.

Supplementary Material

Refer to Web version on PubMed Central for supplementary material.

Acknowledgments

Authors acknowledge financial support from the National Institute of Arthritis and Musculoskeletal and Skin Diseases (NIAMS) and National Institute of Dental and Craniofacial Research (NIDCR) of the National Institutes of Health, USA under Award Number R01 AR066361 and R01 DE029204 respectively. The content is solely the authors' responsibility and does not necessarily represent the National Institutes of Health's official views.

References

[1]. Halvarsson A, Seth M, Tegern M, Broman L, Larsson H, Remarkable increase of musculoskeletal disorders among soldiers preparing for international missions–comparison between 2002 and 2012, BMC Musculoskelet. Disord. 20 (1) (2019) 444.

[2]. Vu AA, Bose S, Vitamin D_3 release from traditionally and additively manufactured tricalcium phosphate bone tissue engineering scaffolds, Ann. Biomed. Eng 48 (2020) 1025–1033. [PubMed: 31168676]

[3]. Laurencin C, Khan Y, El-Amin SF, Bone graft substitutes, Expert Rev. Med. Devices 3 (1) (2006) 49–57.

[4]. Pneumaticos SG, Triantafyllopoulos GK, Basdra EK, Papavassiliou AG, Segmental bone defects: from cellular and molecular pathways to the development of novel biological treatments, J. Cell. Mol. Med 14 (11) (2010) 2561–2569. [PubMed: 20345845]

[5]. Bergmann C, Lindner M, Zhang W, Koczur K, Kirsten A, Telle R, Fischer H, 3D printing of bone substitute implants using calcium phosphate and bioactive glasses, J. Eur. Ceram. Soc 30 (12) (2010) 2563–2567.

[6]. Murugan R, Ramakrishna S, Bioresorbable composite bone paste using polysaccharide based nano hydroxyapatite, Biomaterials 25 (17) (2004) 3829–3835. [PubMed: 15020158]

[7]. Webster TJ, Ergun C, Doremus RH, Siegel RW, Bizios R, Enhanced functions of osteoblasts on nanophase ceramics, Biomaterials 21 (17) (2000) 1803–1810. [PubMed: 10905463]

[8]. Bose S, Vahabzadeh S, Bandyopadhyay A, Bone tissue engineering using 3D printing, Mater. Today 16 (12) (2013) 496–504.

[9]. Koski C, Bose S, Effects of amylose content on the mechanical properties of starch-hydroxyapatite 3D printed bone scaffolds, Addit. Manuf. 30 (2019), 100817.

[10]. Koski C, Onuike B, Bandyopadhyay A, Bose S, Starch-hydroxyapatite composite bone scaffold fabrication utilizing a slurry extrusion-based solid freeform fabricator, Addit. Manuf. 24 (2018) 47–59.

[11]. Jallot E, Benhayoune H, Kilian L, Irigaray J, Barbotteau Y, Balossier G, Bonhomme P, Dissolution kinetics, selective leaching, and interfacial reactions of a bioglass coating enriched in alumina, J. Colloid Interface Sci 233 (1) (2001) 83–90. [PubMed: 11112309]

[12]. Jones JR, Review of bioactive glass: from Hench to hybrids, Acta Biomater. 9 (1) (2013) 4457–4486. [PubMed: 22922331]

[13]. Miguez-Pacheco V, Hench LL, Boccaccini AR, Bioactive glasses beyond bone and teeth: emerging applications in contact with soft tissues, Acta Biomater. 13 (2015) 1–15. [PubMed: 25462853]

[14]. Fagerlund S, Ek P, Hupa L, Hupa M, Dissolution kinetics of a bioactive glass by continuous measurement, J. Am. Ceram. Soc 95 (10) (2012) 3130–3137.

[15]. Ramay HR, Zhang M, Biphasic calcium phosphate nanocomposite porous scaffolds for load-bearing bone tissue engineering, Biomaterials 25 (21) (2004) 5171–5180. [PubMed: 15109841]

[16]. Yang S, Leong K-F, Du Z, Chua C-K, The design of scaffolds for use in tissue engineering. Part II. Rapid prototyping techniques, Tissue Eng. 8 (1) (2002) 1–11. [PubMed: 11886649]

[17]. Tarafder S, Balla VK, Davies NM, Bandyopadhyay A, Bose S, Microwave-sintered 3D printed tricalcium phosphate scaffolds for bone tissue engineering, J. Tissue Eng. Regen. Med 7 (8) (2013) 631–641. [PubMed: 22396130]

[18]. Balla VK, Bose S, Bandyopadhyay A, Understanding compressive deformation in porous titanium, Philos. Mag. 90 (22) (2010) 3081–3094.

[19]. Najafinezhad A, Abdellahi M, Nasiri-Harchegani S, Soheily A, Khezri M, Ghayour H, On the synthesis of nanostructured akermanite scaffolds via space holder method: the effect of the spacer size on the porosity and mechanical properties, J. Mech. Behav. Biomed. Mater 69 (2017) 242–248. [PubMed: 28107739]

[20]. Frayssinet P, Mathon D, Lerch A, Autefage A, Collard P, Rouquet N, Osseointegration of composite calcium phosphate bioceramics, J. Biomed. Mater. Res. Off. J. Soc. Biomater. Jpn. Soc. Biomater. Aust. Soc. Biomater. Korean Soc. Biomater 50 (2) (2000) 125–130.

[21]. Seidenstuecker M, Kerr L, Bernstein A, Mayr HO, Suedkamp NP, Gadow R, Krieg P, Hernandez Latorre S, Thomann R, Syrowatka F, 3D powder printed bioglass and β-tricalcium phosphate bone scaffolds, Materials 11 (1) (2018) 13.

[22]. Ke D, Bose S, Effects of pore distribution and chemistry on physical, mechanical, and biological properties of tricalcium phosphate scaffolds by binder-jet 3D printing, Addit. Manuf. 22 (2018) 111–117.

[23]. Chen QZ, Thompson ID, Boccaccini AR, 45S5 Bioglass®-derived glass–ceramic scaffolds for bone tissue engineering, Biomaterials 27 (11) (2006) 2414–2425. [PubMed: 16336997]

[24]. Oyane A, Kim HM, Furuya T, Kokubo T, Miyazaki T, Nakamura T, Preparation and assessment of revised simulated body fluids, J. Biomed. Mater. Res. Part A Off. J. Soc. Biomater. Jpn. Soc. Biomater. Aust. Soc. Biomater. Korean Soc. Biomater 65 (2) (2003) 188–195.

[25]. Dittler ML, Unalan I, Grünewald A, Beltrán AM, Grillo CA, Destch R, Gonzalez MC, Boccaccini AR, Bioactive glass (45S5)-based 3D scaffolds coated with magnesium and zinc-loaded hydroxyapatite nanoparticles for tissue engineering applications, Colloids Surf. B Biointerfaces 182 (2019), 110346. [PubMed: 31325780]

[26]. Filgueiras MR, La Torre G, Hench LL, Solution effects on the surface reactions of a bioactive glass, J. Biomed. Mater. Res 27 (4) (1993) 445–453. [PubMed: 8385143]

[27]. Ginebra M-P, Fernandez E, De Maeyer E, Verbeeck R, Boltong M, Ginebra J, Driessens F, Planell J, Setting reaction and hardening of an apatitic calcium phosphate cement, J. Dent. Res 76 (4) (1997) 905–912. [PubMed: 9126187]

[28]. Motisuke M, Carrodeguas RG, Ad C. Zavaglia C, Si-TCP synthesized from“ Mg-free” reagents employed as calcium phosphate cement, Mater. Res 15 (4) (2012) 568–572.

[29]. Paluszkiewicz C, Blażewicz M, Podporska J, Gumuła T, Nucleation of hydroxyapatite layer on wollastonite material surface: FTIR studies, Vib. Spectrosc. 48 (2) (2008) 263–268.

[30]. Fraga AF, de Almeida Filho E, da Silva Rigo EC, Boschi AO, Synthesis of chitosan/hydroxyapatite membranes coated with hydroxycarbonate apatite for guided tissue regeneration purposes, Appl. Surf. Sci 257 (9) (2011) 3888–3892.

[31]. Teixeira S, Rodriguez M, Pena P, De Aza A, De Aza S, Ferraz M, Monteiro F, Physical characterization of hydroxyapatite porous scaffolds for tissue engineering, Mater. Sci. Eng. C 29 (5) (2009) 1510–1514.

[32]. Will J, Melcher R, Treul C, Travitzky N, Kneser U, Polykandriotis E, Horch R, Greil P, Porous ceramic bone scaffolds for vascularized bone tissue regeneration, J. Mater. Sci. Mater. Med 19 (8) (2008) 2781–2790. [PubMed: 18305907]

[33]. Vu AA, Burke DA, Bandyopadhyay A, Bose S, Effects of surface area and topography on mechanical properties of 3D printed tricalcium phosphate scaffolds for osteoblast proliferation in bone grafting applications, Addit. Manuf. (2021), 101870.

[34]. Lin K, Chen L, Qu H, Lu J, Chang J, Improvement of mechanical properties of macroporous β-tricalcium phosphate bioceramic scaffolds with uniform and interconnected pore structures, Ceram. Int 37 (7) (2011) 2397–2403.

[35]. Jones JR, Sepulveda P, Hench LL, Dose-dependent behavior of bioactive glass dissolution, J. Biomed. Mater. Res. Off. J. Soc. Biomater. Jpn. Soc. Biomater. Aust. Soc. Biomater. Korean Soc. Biomater 58 (6) (2001) 720–726.

[36]. Bandyopadhyay A, Bernard S, Xue W, Bose S, Calcium phosphate-based resorbable ceramics: influence of MgO, ZnO, and SiO_2 dopants, J. Am. Ceram. Soc 89 (9) (2006) 2675–2688.

[37]. Sanz-Herrera J, Boccaccini A, Modelling bioactivity and degradation of bioactive glass based tissue engineering scaffolds, Int. J. Solids Struct 48 (2) (2011) 257–268.

[38]. Bohner M, Lemaître J, Ring TA, Kinetics of dissolution of β-tricalcium phosphate, J. Colloid Interface Sci 190 (1) (1997) 37–48. [PubMed: 9241139]

[39]. Oktar FN, Goller G, Sintering effects on mechanical properties of glass-reinforced hydroxyapatite composites, Ceram. Int 28 (2002) 617–621.

[40]. Baino F, Caddeo S, Vitale-Brovarone C, Sintering effects of bioactive glass incorporation in tricalcium phosphate scaffolds, Mater. Lett 274 (2020), 128010.

[41]. Lopes JH, Magalhaes JA, Gouveia RF, Bertran CA, Motisuke M, Camargo SEA, Triches ES, Hierarchical structures of β-TCP/45S5 bioglass hybrid scaffolds prepared by gel casting, J. Mech. Behav. Biomed. Mater 62 (2016) 10–23. [PubMed: 27161958]

[42]. German RM, Suri P, Park SJ, liquid phase sintering, J. Mater. Sci 44 (1) (2009) 1–39.

[43]. Kaur G, Kumar V, Baino F, Mauro JC, Pickrell G, Evans I, Bretcanu O, Mechanical properties of bioactive glasses, ceramics, glass-ceramics and composites: state-of-the-art review and future challenges, Mater. Sci. Eng. C 104 (2019), 109895.

[44]. Filho OP, La Torre GP, Hench LL, Effect of crystallization on apatite-layer formation of bioactive glass 45S5, J. Biomed. Mater. Res. J. Soc. Biomater. Jpn. Soc. Biomater 30 (1996) 509–514.

[45]. Ker CA, Kah FL, Chee KC, Margam C, Investigation of the mechanical properties and porosity relationships in fused deposition modelling-fabricated porous structures, Rapid Prototyp. J 12 (2006) 100–105.

[46]. Sudarmadji N, Tan JY, Leong KF, Chua CK, Loh YT, Investigation of the mechanical properties and porosity relationships in selective laser-sintered polyhedral for functionally graded scaffolds, Acta Biomater 7 (2011) 530–537. [PubMed: 20883840]

[47]. Tarafder S, Banerjee S, Bandyopadhyay A, Bose S, Electrically polarized biphasic calcium phosphates: adsorption and release of bovine serum albumin, Langmuir 26 (2010) 16625–16629. [PubMed: 20939493]

[48]. Pietak AM, Reid JW, Stott MJ, Sayer M, Silicon substitution in the calcium phosphate bioceramics, Biomaterials 28 (2007) 4023–4032. [PubMed: 17544500]

[49]. Robertson SF, Bose S, Enhanced osteogenesis of 3D printed β-TCP scaffolds with Cissus quadrangularis extract-loaded polydopamine coatings, J. Mech. Behav. Biomed. Mater 111 (2020), 103945. [PubMed: 32920263]

[50]. Osidak EO, Kozhukhov VI, Osidak MS, Domogatsky SP, Collagen as bioink for bioprinting: a comprehensive review, Int. J. Bioprint 6 (2020) 270. [PubMed: 33088985]

[51]. Lee JM, Suen SKQ, Ng WL, Ma WC, Yeong WY, Bioprinting of collagen: considerations, potentials, and applications, Macromol. Biosci. 21 (2021), 2000280.

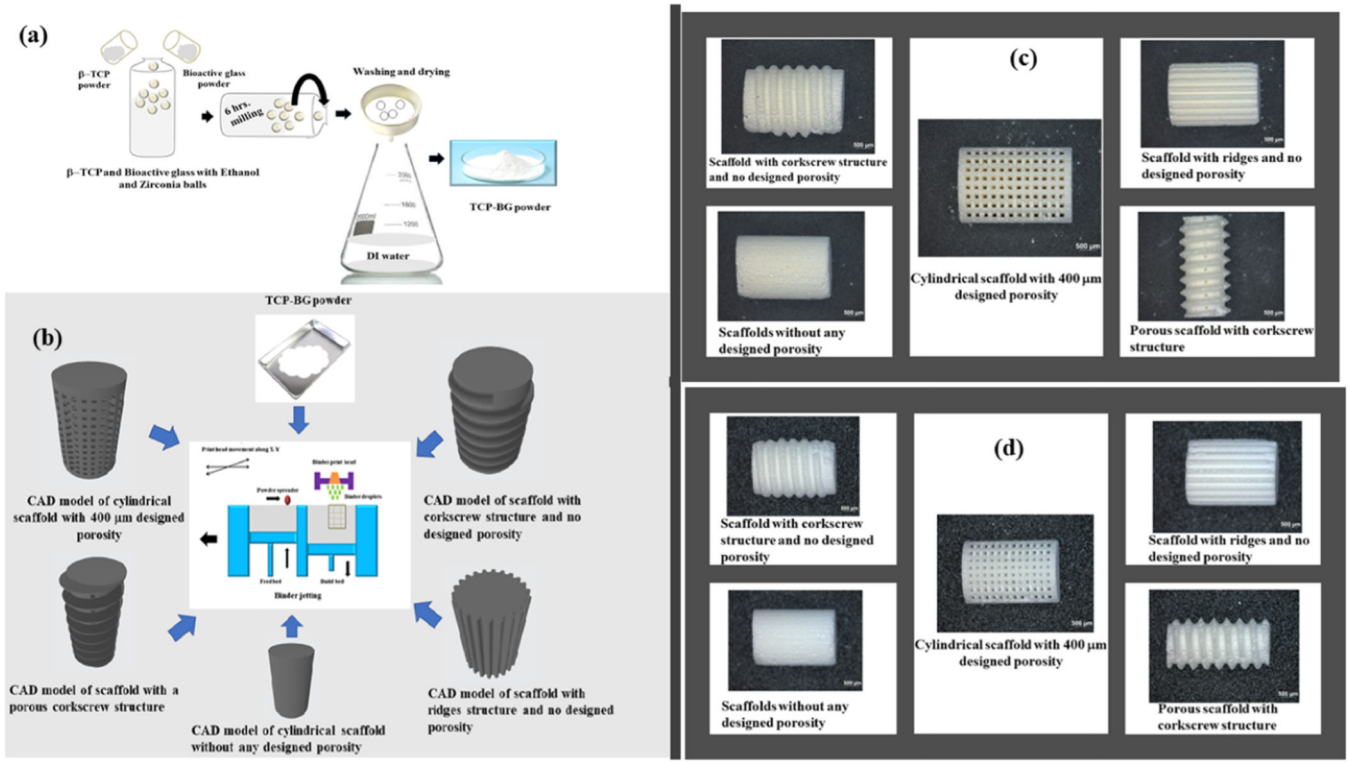

Fig. 1.

(a) Synthesis method of TCP-BG powders using the β–TCP and Bioactive glass powders as precursors, (b) Illustration of binder jetting method for fabricating TCP-BG scaffolds using the CAD models with five different designs: cylindrical scaffold with 400 µm porosity, scaffold with corkscrew structure and no designed porosity, scaffold with ridges structure and no designed porosity, cylindrical scaffold without any designed porosity, and scaffold with a porous corkscrew structure. (c) Binder-jet 3D printed green scaffolds with different designs, and (d) Obtained scaffolds after sintering at 1250 °C with 2 h holding.

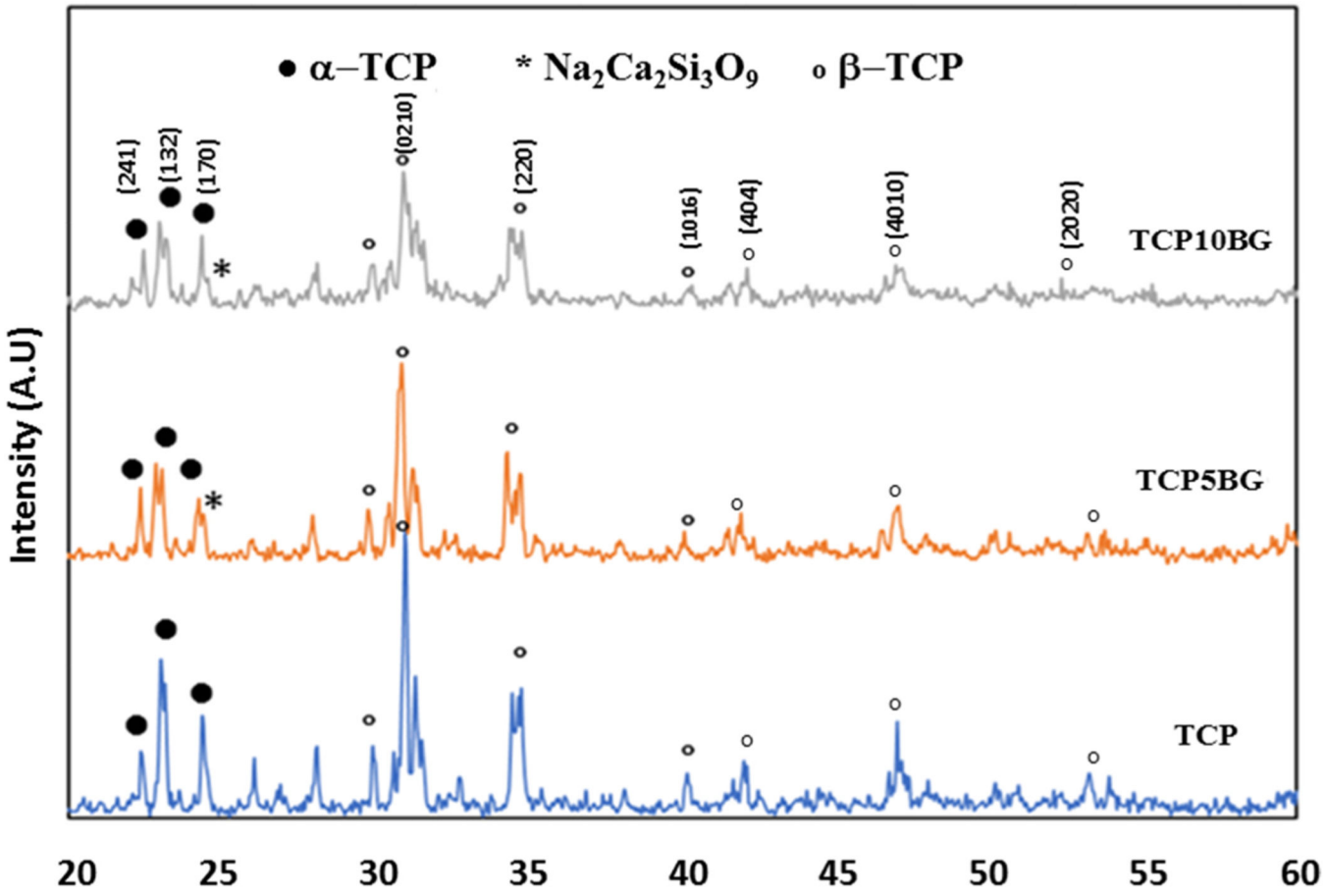

Fig. 2.

XRD spectra of TCP and BG added TCP powders. The presence of $Na_2Ca_2Si_3O_9$, and TCP phases are confirmed from the spectra.

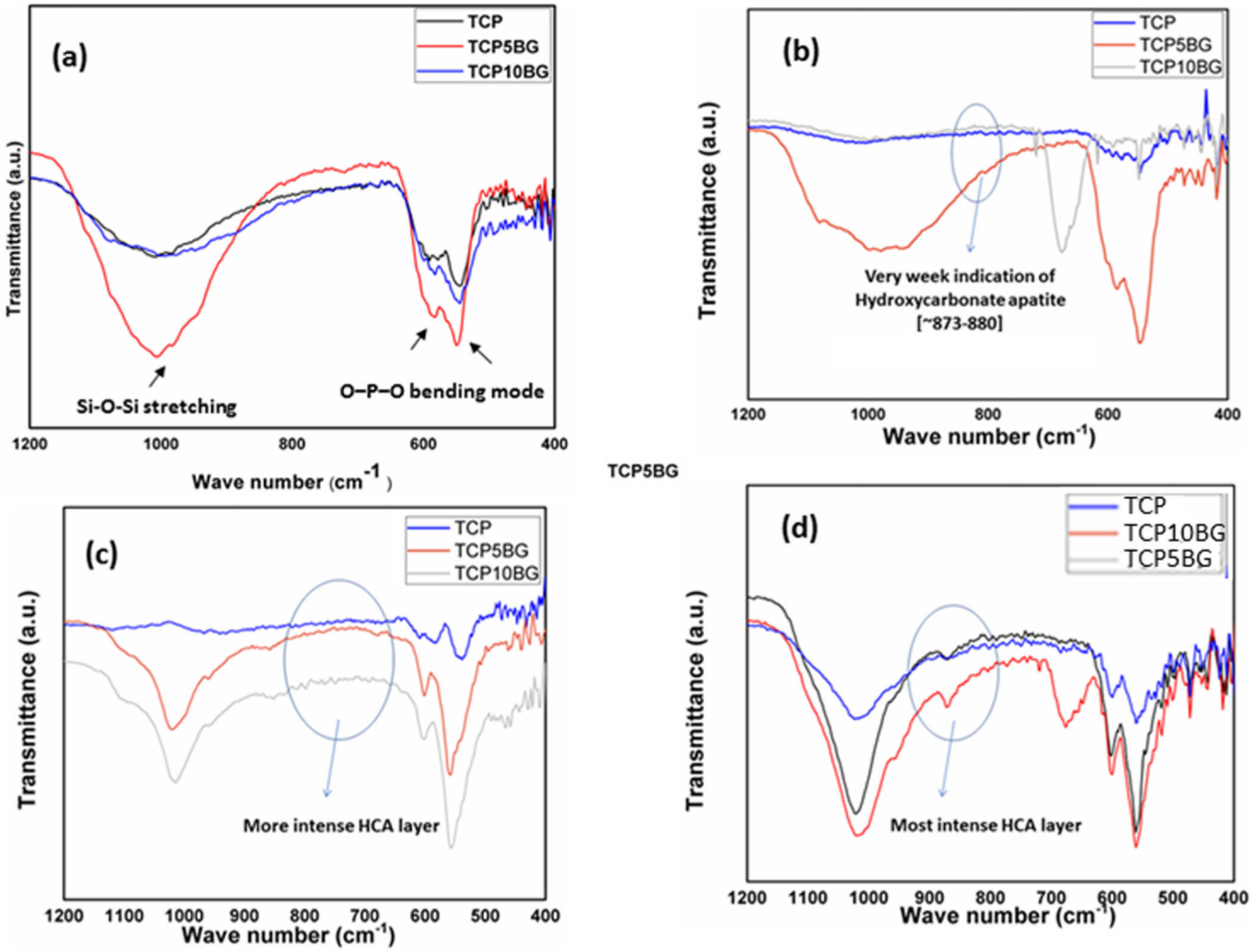

Fig. 3.

ATR-IR spectra of (a) TCP- BG powders, bands corresponding to both BG and TCP phases are observed in the range 400–1200 cm^{-1} (b) after 1-week dissolution (c) after 4 weeks dissolution, and (d) after 8 weeks dissolution in SBF. The intensity of the hydroxycarbonate apatite layer increases with dissolution time and the amount of BG addition.

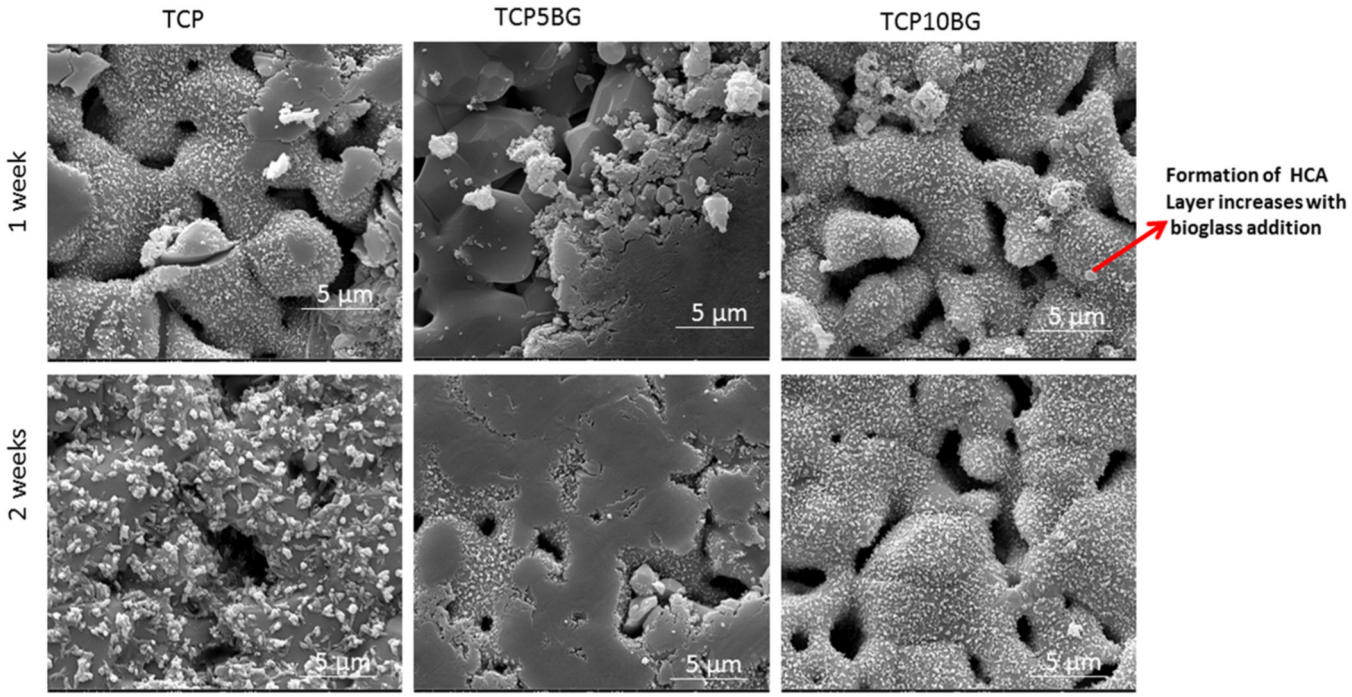

Fig. 4.

SEM images of all samples after 1 and 2 weeks of dissolution. Mild hydroxycarbonate apatite layers are observed and the most intense layer is observed for the 10% BG doped TCP sample.

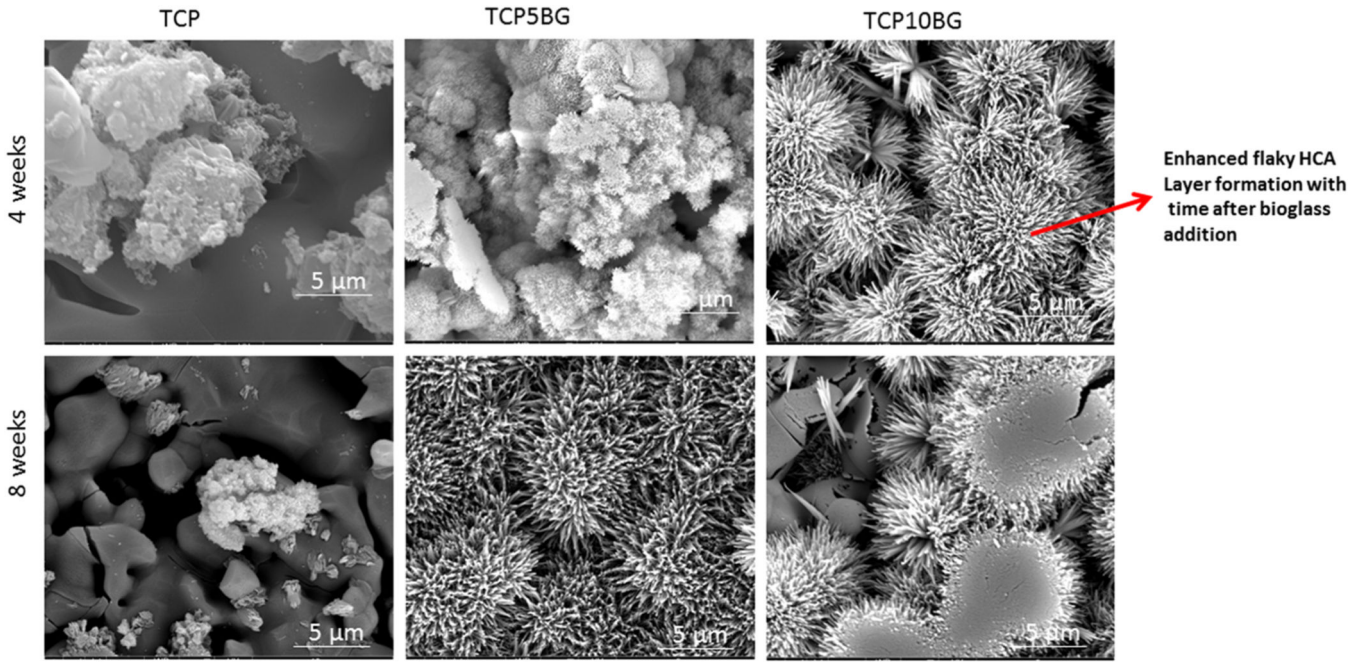

Fig. 5.

SEM images of all samples after 4 and 8 weeks of dissolution. More intense hydroxycarbonate apatite layers are observed as compared to earlier time points, and it increases significantly with BG addition.

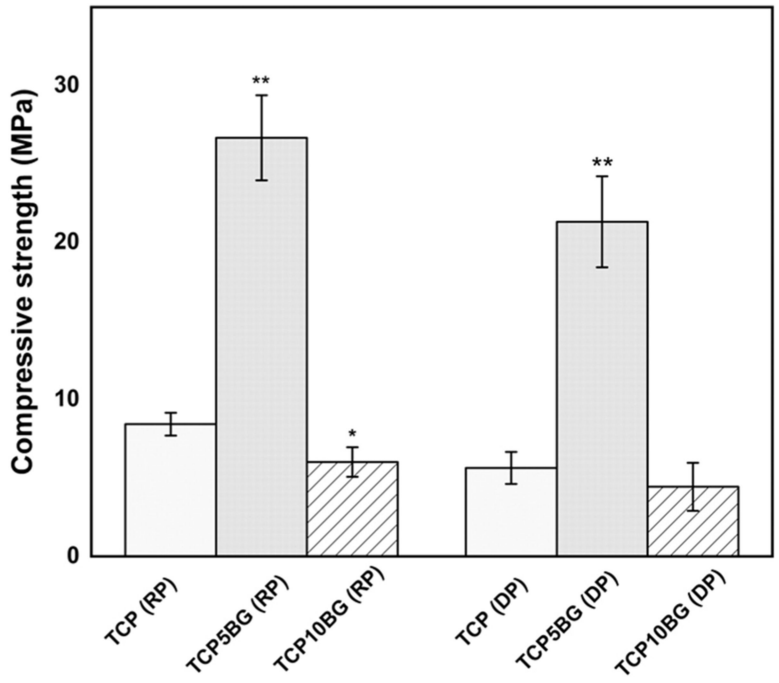

Fig. 6.

Compressive strength of prepared randomly porous (RP) and designed porous (DP) scaffolds (n = 6). BG addition upto 5 wt% significantly increases the compressive strength to 26.7 ± 2.7 MPa as compared to 8.42 ± 0.73 MPa of randomly porous TCP. A similar trend is shown after introducing designed porosity. Statistical analysis of obtained data is performed by student's *t*-test (* $p < 0.05$; ** $p < 0.005$).

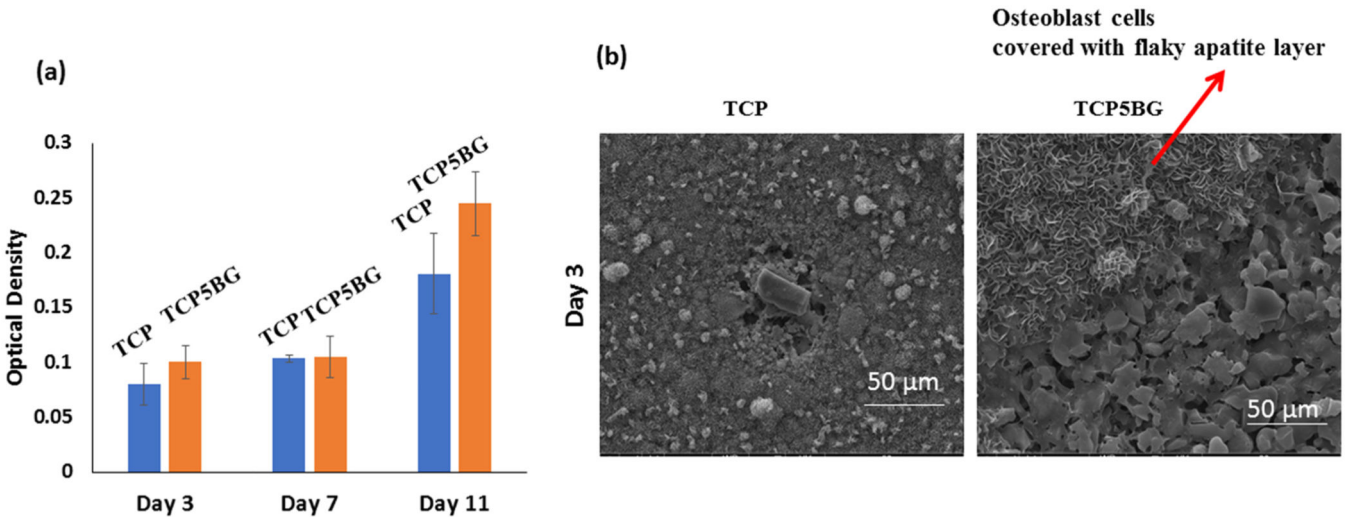

Fig. 7.

Cytotoxicity assessment (a) Osteoblast cell viability by MTT assay, (b) SEM images at a 3-day time point after cell-material interaction. MTT assay shows no significant decrease in cell viability after bioactive glass addition than control TCP, proving the tested compositions' cytocompatibility.

Table 1

3DP process parameter optimization for printing TCP-BG scaffolds.

Layer thickness (μm)	Binder saturation (%)	Drying time between consecutive printing layers (seconds)	Outcome
30	78	2	Crumbled powder
35	78	2	Layer displaced scaffolds with cracks
35	70	5	A lot of layer displacement
40	72	5	Relatively little layer displacement, run stopped twice in between
40	70	5	Perfect scaffolds for further characterization

Table 2

Bulk density, total porosity, relative bulk density, open porosity, designed porosity, volume shrinkage, and calculated compressive strength of scaffolds with random and designed porosity.

Sample	Bulk density (g/ cm^3)	Total porosity (%)	Relative bulk density (%)	Open porosity (%)	Designed porosity (%)	Volume shrinkage after sintering (%)	Calculated compressive strength (MPa)
TCP (DP)	1 ± 0.06	68.3 ± 0.02	31.6 ± 0.04	48.2 ± 1.5	42	8.7 ± 1.1	6.1
TCP5BG (DP)	1.4 ± 0.05 **	54.1 ± 0.02 **	45.8 ± 0.03 **	35.5 ± 2.4 *	42	11.6 ± 1 *	16.1
TCP10BG (DP)	0.9 ± 0.04	69.4 ± 0.02 **	30.5 ± 0.02 **	51.8 ± 2.8	42	8.6 ± 0.3	6.3
TCP (RP)	1.1 ± 0.03	62.5 ± 0.01	37.3 ± 0.03	39.4 ± 2.1	–	9.2 ± 0.3	8.3
TCP5BG (RP)	1.6 ± 0.04 **	47.9 ± 0.03 **	52.1 ± 0.02 **	28.9 ± 3.3 *	–	13.7 ± 1.1 *	54.4
TCP10BG (RP)	0.98 ± 0.05 *	67.7 ± 0.02 **	32.1 ± 0.04 **	47 ± 3.8	–	10.9 ± 1.8	5.2

* denotes $p < 0.05$ and

** denotes $p < 0.005$; $n = 6$; (DP) stands for scaffolds with designed porosity and (RP) stands for scaffolds with random porosity, respectively.